Available online at www.sciencedirect.com

jmr&t Journal of Materials Research and Technology

journal homepage: www.elsevier.com/locate/jmrt

Original Article

Innovative X-ray diffraction and micromagnetic approaches for reliable residual stress assessment in deep rolled and microfinished AISI 4140 components

Simon Strodick [a,*], *Florian Vogel* [b], *Meik Tilger* [b], *Marie Denstorf* [b], *Monika Kipp* [b], *Nikolas Baak* [a], *Dimitri Kukui* [a], *Dirk Biermann* [b], *Marina Macias Barrientos* [a], *Frank Walther* [a]

[a] *TU Dortmund University, Chair of Materials Test Engineering, Baroper Str. 303, 44227 Dortmund, Germany*
[b] *TU Dortmund University, Institute of Machining Technology, Baroper Str. 303, 44227 Dortmund, Germany*

ARTICLE INFO

Article history:
Received 25 May 2022
Accepted 29 July 2022
Available online 3 August 2022

Keywords:
Residual stresses
Surface integrity
Deep rolling
Microfinishing
cos α X-ray diffraction
$\sin^2 \psi$ X-ray diffraction
Magnetic Barkhausen noise

ABSTRACT

The residual stress state in the subsurface is a key element of surface integrity. It is well known to have a significant impact on a component's properties in terms of fatigue behavior and resistance to wear and corrosion. For this reason, adjusting residual stresses during manufacturing is a major challenge in modern production engineering, to improve and ensure a component's fatigue strength. In this context, hydrostatic deep rolling of the workpiece surface using adapted parameters enables the targeted induction of compressive residual stresses into subsurface layers. Due to specific properties regarding subsurface and topography for functional components in tribological applications, a further machining operation by microfinishing following deep rolling seems to be purposeful. In particular with regard to the production of components exposed to periodic load changes when used, the process combination can enable a substitution of the typically required conventional subsurface zone hardening. With the aim of economical process design, the corresponding parts can be manufactured with significantly reduced time and costs. Efficient and well-founded methods for monitoring the resulting influence on the subsurface zone properties are essential for a reproducible and target-oriented process design. The prevailing method for the non-destructive assessment of residual stresses in both academia and industry is X-ray diffractometry using the $\sin^2 \psi$-method. However, this method is time-intensive and requires complex instrumentation. Thus, efforts have been undertaken in past decades to develop alternative methods for the efficient and reliable characterization of residual stresses. In this research, the applicability of the cos α-method in X-ray diffractometry and a micromagnetic approach for residual stress assessment was investigated, analyzing deep rolled and microfinished AISI 4140 specimen conditions. In addition to the diffractometric and micromagnetic measurements, metallographic and topographic analyses of machined surfaces were carried out. Deep rolling was found to induce significant compressive residual stresses of up to −1100 MPa. After microfinishing

* Corresponding author.
E-mail address: simon.strodick@tu-dortmund.de (S. Strodick).
https://doi.org/10.1016/j.jmrt.2022.07.168

of the deep rolled surfaces, favorable compressive residual stresses remain in the subsurface, reaching approximately up to −750 MPa. Based on this, the production of tailored surfaces with respect to a suitable combination of topography and subsurface is possible. For all surface states investigated, a good agreement between the two approaches in X-ray diffraction was found. Magnetic Barkhausen noise (MBN) measurements prove to be well applicable for an efficient and holistic assessment of surface integrity in the subsurface of deep rolled and microfinished AISI 4140 specimens.

1. Introduction

Favorable compressive residual stresses generally improve fatigue resistance by postponing the initiation and growth of cracks, whereas tensile residual stresses have an impairing effect on fatigue capability [1]. The precise assessment of residual stresses and the targeted induction of compressive residual stresses in manufacturing processes have thus become crucial fields of research in modern production engineering. Depending on the context, different factors dominate the decision for a particular measurement method when it comes to the assessment of residual stresses. In industrial contexts, often the time efficiency and reliability of measurements are decisive factors, whereas in academia there is a high demand for in-depth measurements which allow analyzing underlying mechanisms of the induction of residual stresses. In this research, two diffractometric approaches and a micromagnetic method were assessed to qualify cos α-method in X-ray diffractometry and the analysis of magnetic Barkhausen noise as innovative and time-saving methods for reliable residual stress assessment.

The most widespread non-destructive method for characterizing residual stresses is X-ray diffractometry and the mainly employed experimental method is the $\sin^2 \psi$-method [2]. An alternative is the cos α-method. Both methods share as their fundamental principle the detection of diffracted X-rays according to Bragg's law. This way elastic lattice strains, resulting from residual stresses inside a material, can be characterized and used to calculate the stresses near the surface. In $\sin^2 \psi$-method, the diffracted X-rays are measured for various ψ-inclinations oftentimes using line or point detectors. Using such a setup, the diffraction cone is observed for the maximum at two radii. Due to the required ψ-inclinations, the method tends to be time-intensive and requires complex instrumentation. In addition to this, performing measurements according to the $\sin^2 \psi$-method demands meticulous attention to detail, a relatively high level of knowledge of the operator, and specialist skills, due to the complexity of instrumentation. Cos α-method was developed in Japan in the late 1970s, based on the first measurements of lattice strains using X-ray diffraction performed by Peter Debye and Paul Scherrer in the early days of X-ray diffraction at the beginning of the 20th century [3,4]. In contrast to $\sin^2 \psi$-method, it is based on the analysis of a single diffracted Debye–Scherrer cone. Residual stresses inside a material cause a characteristic deformation of the cone. The deformed cone detected is compared to the undeformed cone of the stress-free state to calculate residual stresses. Thus, this method relies on state-of-the-art two-dimensional detectors [4]. Due to the increasing quality of these components in the past decades, this method has lately been gaining importance, yet it is not widely spread and almost exclusively used in academic contexts. To obtain depth profiles of the residual stresses inside a material, XRD measurements can be performed intermittently in combination with electrochemical machining. In contrast to mechanical methods for material removal, electrochemical machining does not alter the residual stress state. A major downside of this method is the partial destruction of the workpiece. Non-destructive methods for obtaining depth-resolved residual stresses include the use of conical slits [5], synchrotron X-rays [6] and neutron diffraction [7,8]. These elaborate methods, however, are marked by great complexity and thus are usually not attractive in industrial contexts and oftentimes only used when other, less complex methods cannot be used [8].

Due to the many drawbacks of X-ray diffractometry, sustained efforts have been undertaken in the past decades to investigate the applicability of easy-to-apply micromagnetic methods for the fast and reliable characterization of residual stresses in the subsurface of specimens. The most established method in this field is the analysis of magnetic Barkhausen noise (MBN). MBN is a method for the non-destructive assessment of material properties based on the analysis of magnetic properties. When a ferromagnetic material is subjected to an external periodically changing magnetic field, the internal flux changes accordingly. This change does not occur linearly but in discrete jumps, called Barkhausen jumps. When the coercive field strength is applied, the intensity of these jumps reaches its maximum M_{max}. The intensity of Barkhausen jumps in MBN analysis is influenced by various properties of the material, like grainsize, hardness and the residual stress state [9–12]. Thus, MBN analysis generally is applicable for characterizing all of these properties in subsurface. However, due to the multitude of factors that have an impact on MBN, a key challenge in MBN analysis is to separate the effects of the aforementioned properties, which is not always possible and requires extensive calibration efforts. In addition to this, the assessment of the depth of analysis in micromagnetic testing poses a demanding challenge and MBN analysis is only applicable for characterizing ferromagnetic materials. The most prominent application of MBN in industrial contexts is the detection of grinding burn as an alternative to nital etching [11]. Due to the many advantages of the method, particularly its time efficiency, persistent efforts have been undertaken to expand the industrial use of MBN to other applications [10–13].

Deep rolling is an established process that has been used since the beginning of the 20th century to substantially increase the fatigue strength of dynamically loaded metallic workpieces by elastic-plastic forming processes of surface and subsurface layers [14–16]. The reduction of pronounced roughness peaks and the resulting material flow on the one hand lead to the induction of compressive residual stresses in the subsurface layers and simultaneous work hardening of those layers with a significant increase in their hardness. On the other hand, the reduction in surface roughness is accompanied by an elimination of micro notches, which are considered to be a nucleus for crack formation damages [15,17,18]. In combination with the induced compressive residual stresses, the improved surface quality resulting from deep rolling also contributes to an increased thermal fatigue strength [19]. A detailed account of the complex interrelations between the flow of material in deep rolling and the resulting residual stress state can be found in [20]. With respect to influencing the subsurface layers, deep rolling is comparable with alternative surface treatment processes such as shot-peening. However, the maxima of the compressive residual stresses induced during deep rolling can be observed in much deeper layers [14,17,21]. The primary parameter influencing the results of deep rolling processes is the deep rolling force, respectively the rolling pressure set when using hydrostatic deep rolling tools. Basically, it can be observed that the induced compressive residual stresses also rise by increasing the deep rolling force [14,22,23]. However, it must be taken into account that as soon as the deep rolling force exceeds a material-specific limit, the maxima of the induced compressive residual stresses are shifted to deeper layers and tensile stresses may occur in the subsurface area [14]. Further process parameters influencing the properties of the surface and subsurface layers are the rolling speed, the rolling feed, the diameter of the used rolling element and the number of passes [15,16,23]. In this context, it could be identified that generally, the highest possible value of the induced compressive residual stresses is already achieved during the first rolling operation and that further passes may even reduce this maximum value [16]. Since further investigations have also shown that the number of passes is an overall factor that not only affects the residual stress level, the associated interactions should be considered as a central focal point of subsequent investigations [18,24,25].

Microfinishing, also known as superfinishing or precisely called short-stroke honing is typically used as the last step in the production chain to create functional surfaces for tribologically loaded applications, e.g. bearing surfaces [26–28]. According to the ISO standard, microfinishing is a cutting process with geometric undefined cutting edge. The characteristic cross-grid patterned topography is created by the rotation of the workpiece and the orthogonal oscillation of the tool. The tool consists of microfinishing stones or flexible belts with bonded cutting grains using aluminia (Al_2O_3), Diamond (D), silicium carbide (SiC) or cubic boron nitride (cBN). Using belts for microfinishing a pressure roll is used to guide the belt and press it against the workpiece with a constant pressure [28]. The microfinishing process is usually carried out in several stages, whereby the material removal decreases from stage to stage as the used tool's grain size is smaller within every subsequent stage. The stages typically start with a large grain size, up to $d_K = 125$ μm. Further, the grain orientation often is changed from electrostatically oriented to gravity-scattered grain distribution. It is therefore possible to create plateau-structured topographies without profile peaks, which is favorable for tribological functions of components [27–29]. Due to the first process stage, relatively deep grooves are machined, whereby peaks occur caused by the interacting material removal mechanisms microcracking and microfatigue, and mechanisms of microridging, microploughing, and microcutting, which can lead to lateral bulges [27,30–34]. The further process stages using smaller grain sizes and gravity-scattered grain distribution lead to a removal of the peaks by cutting these bulges [27,30–35]. Furthermore, it is known that microfinishing with abrasive belts does not lead to high temperatures and thus combined with the force-controlled process kinematic explains why it typically leads to compressive residual stresses [36,37].

Due to the mentioned specific characteristics of both production processes concerning the subsurface properties and topography, a combination of both processes is promising to lead to targeting properties for functional components in tribological applications. Unlike grinding processes, finishing operations affect only a small layer near the surface [26]. Moreover, no thermal damage of the subsurface is to be expected [26]. Therefore, it is assumed that there is only a minor influence of the microfinishing on the compressive residual stresses caused by the deep rolling operation, whereby a surface topography with plateau-structure could be created. Since each process combination leads to specific properties of the workpiece, it is essential to gain knowledge about the interactions of the deep rolling and microfinishing processes. For this reason, the conducted investigations focus on the residual stress state, topography and material removal depending on different process steps.

2. Materials and methods

2.1. Preparation of the specimens

2.1.1. Materials and pre-processing

All experiments were carried out for AISI 4140 (DIN 1.7225, 42CrMo4) in a quenched and tempered (+QT) state. The chemical composition is given in Table 1, the mechanical properties in Table 2. All batches used meet the standard

Table 1 – Chemical composition of AISI 4140+QT investigated (mass fraction in %).

Specimen	C	Mn	Si	P	S	Cr	Ni	Mo	Cu	Fe
Type A	0.40	0.76	0.22	0.016	0.025	1.05	0.08	0.16	0.11	bal.
Type B	0.41	0.82	0.24	0.021	0.031	1.11	0.02	0.21	0.03	bal.

Table 2 – Mechanical properties of AISI 4140+QT investigated.

Specimen	$R_{p\ 0,2}$ in MPa	R_m in MPa	A in %	Z in %
Type A	1038	1108	19.0	59
Type B	892	1013	17.0	58

according to EN 10083-3. Two specimen geometries were chosen for the analyses in this study, optimized for the particular measuring tasks (Fig. 1). Specimens of type A were designed for the use in extensive fatigue tests, which will follow this study. Figure 1 (a) depicts the center of these specimens for the different surface treatment stages. In addition to this, an optimized specimen geometry for residual stress tests was employed, which exhibits various, differently machined areas for each specimen (type B). For this purpose, it was first necessary to pre-process the specimens by turning in order to achieve the required specimen design and related to this to enable the subsequent processing steps according to the experimental design. The relevant turning parameters used are summarized in Table 3. Regarding the subsequent processes, the areas 1, 2 and 3 were subjected to deep rolling and microfinishing, whereas the area marked with 4 was only subjected to deep rolling (Fig. 1). This design was chosen to investigate the impact of deep rolling and microfinishing on the residual stress state and on the microstructure in the subsurface.

2.1.2. *Deep rolling*

The first part of the preparation process of the specimens, the deep rolling, was carried out on a CNC lathe of the Monforts company (type "RNC 602″). For this purpose, the workpieces made of AISI 4140+QT were clamped in the machine's three-jaw chuck and additionally supported by the tailstock quill (Fig. 2). The pre-machining was carried out with indexable inserts of the type "VBMT160404-F1″ from Seco Tools GmbH using a cutting velocity of $v_c = 150$ m/min, a feed of $f_c = 0.15$ mm, a depth of cut of $a_p = 0.20$ mm and a conventional coolant supply. The pressure required for deep rolling was generated by an external hydraulic unit filled with 6% emulsion. This hydraulic unit and also the hydrostatic deep rolling tools used were produced by ECOROLL AG. The tool applied for deep rolling the specimens for the residual stress measurements only had a single rolling element with a ball diameter of $d_b = 6$ mm (Fig. 2, bottom left). In contrast, a tool with three rolling elements of the same ball diameter directed towards the workpiece's center was used for deep rolling the contoured fatigue strength test specimens (Fig. 2, bottom right).

The advantage of using a tool with three deep rolling balls, each offset by 120°, is that the fatigue strength test specimens with comparatively small diameters are automatically supported during the rolling process, thus preventing displacement of the workpiece. Corresponding to the three rolling elements, the feed rate for deep rolling with this tool had to be three times higher than the feed rate used for rolling with a single rolling element to ensure comparability of the respective deep rolling processes. In order to further analyze the influence of multiple deep rolling cycles on the workpiece properties the number of passes was varied for both specimen types. This way potential effects of multiple deep rolling passes in combination with the subsequent microfinishing process were identified. An overview of all parameters used for deep rolling is shown in Table 4.

2.1.3. *Finishing*

The second part of the preparation process of the specimens is microfinishing and was carried out on a cylindrical grinding machine from Geibel & Hotz GmbH, Germany (type: RS 600 C CL) with an integrated microfinishing unit (Fig. 3). The microfinishing unit type NBFG 5 from Nagel Maschinen-und Werkzeugfabrik GmbH, Germany was used. The microfinishing belt and the pressure roll are implemented into the microfinishing unit. The belt movement “belt feed speed”, the

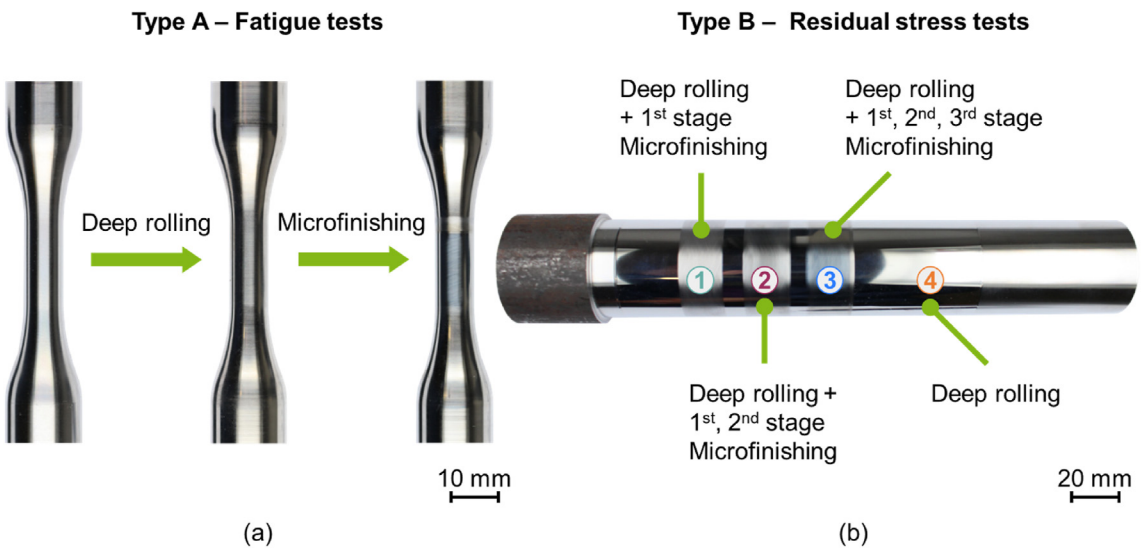

Fig. 1 – Surface treatment: (a) specimens of type A for fatigue tests; (b) specimens of type B for residual stress tests.

Table 3 – Used turning parameters for pre-processing the specimens.

Specimen	Tool	Cutting velocity v_c	Feed f	Depth of cut a_p	Lubricant
Type A	VBMT160404-F1	150 m·min^{-1}	0.15 mm	0.20 mm	Oil
Type B	CNMG120408-M3	150 m·min^{-1}	0.15 mm	0.20 mm	Emulsion, 6%

tool oscillation and the contact force are applied by the microfinishing unit.

The microfinishing process was carried out through three stages using different grain sizes and cutting times. The grain distribution of the microfinishing belts was gravity-scattered with diamond as an abrasive medium. Due to the fact that the specimens have varying diameters, the normal force Fn was varied. Depending on the measurements of the resulting surface pressure using Fujifilm's prescale measuring film [38], the same resulting surface pressure was determined for both diameters in order to achieve an identical process setting. The parameters used for microfinishing are shown in Table 5.

2.2. Topographic analysis

The topographic analysis was carried out using a confocal white-light microscope by NanoFocus (NanoFocus AG, Oberhausen, Germany) type μsurf C. To create a three-dimensional image of the topography, a 50× magnification lens with a numerical aperture of 0.8 was used. The three-dimensional images were analyzed with the software μsoft Analysis Extended 7 b y DigitalSurf. The roughness of the specimens was measured using the tactile roughness tester MarSurf XR 20 from Mahr (Mahr GmbH, Göttingen, Germany). Based on DIN EN ISO 4288 the roughness measuring were carried out with specific profile length and thus, filtered with the specific cut-off filter λ_c. To investigate the material removal caused through the finishing process, the specimens were analyzed by the tactile contour measuring device MarSurf XC 20.

2.3. Metallographic analysis

Metallographic analysis was performed on the cross-sections of specimens Type B. After X-ray diffractometry and micromagnetic analysis, the specimens were cut and cross-sections taken out in longitudinal direction from each area corresponding to the different surface treatments as shown in Fig. 1 (b). The cross-sections were embedded, grinded, polished and etched with the nital etching solution. A scanning electron microscope FIB-SEM Zeiss, XB 550 L was used to analyze the microstructure of the subsurface.

Table 4 – Parameters used for deep rolling of the two types of specimens.

Type	No.	Rolling velocity v_r in m/min	Feed f_r in mm	Pressure p_r in bar	No. of passes n
Fatigue strength test (Type A)	1	50	0.05	200	1
	2	50	0.05	200	2
	3	50	0.15	200	1
	4	50	0.15	200	2
Residual stress test (Type B)	5	50	0.05	200	1
	6	50	0.05	200	2

2.4. Characterization of the residual stress state

2.4.1. X-ray diffractometry

For the diffractometric analysis of the subsurface macroscopic residual stress state, two measurement devices were used. Bruker D8 Discover (Fig. 4 (a)) (Bruker Corporation, Billerica, US) which assesses residual stresses following the $\sin^2\psi$-method and Pulstec μ-X360s (Fig. 4 (b)) (Pulstec Industrial Corporation, Nakagawa, Japan) which operates according to the cos α-method. The parameters used for the investigations can be found in Table 6. Specimens of type A were assessed using both devices, whereas specimens of type B were analyzed by cos α-method exclusively. The reason is that the weight of the specimens for residual stress tests (type B) exceeded the allowed limit of the Euler's cradle.

Since penetration depth of X-rays mainly depends on the anode material, workpiece material and angle of incidence, these parameters were kept constant for all measurements [2]. Due to their small radii, the specimens of type A were analyzed, using a collimator with a diameter of $d_{col} = 0.3$ mm, whereas a diameter of $d_{col} = 2$ mm was used for the characterization of the specimens of type B, resulting in a spot size of $d_{meas} = 0.6$ mm for type A specimens and $d_{meas} = 4$ mm for type B specimens. The average time for measurements using Pulstec μ-360s was $t \approx 160$ s for type A specimens and $t \approx 45$ s for type B specimens. Using Bruker D8 discover resulted in a time of $t \approx 3$ h 40 min for each measurement. Measurements were performed in axial and tangential direction of the specimens. Depth profiles of the residual stresses were performed by electrochemical machining and intermittent X-ray diffractometry. A key difference in the application of both methods is the design of the system. Whereas the Bruker is a fully radiation protected system with several axes and an Euler's cradle to accurately set the required $\sin^2\psi$ increments, Pulstec is a compact portable system, mounted to a tripod, which can easily be moved around a laboratory (Fig. 4). Even when strict safety/radiation policies need to be met, the low power X-ray output usually allows the system to be used as a portable system (Table 5).

2.4.2. Micromagnetic methods

For the fast characterization of the residual stress state in the subsurface of specimens, micromagnetic measurements are well established in academic context, one commonly used being the analysis of magnetic Barkhausen noise [9–11,13,39]. For the specimens of type B magnetic Barkhausen noise measurements were performed by means of the device

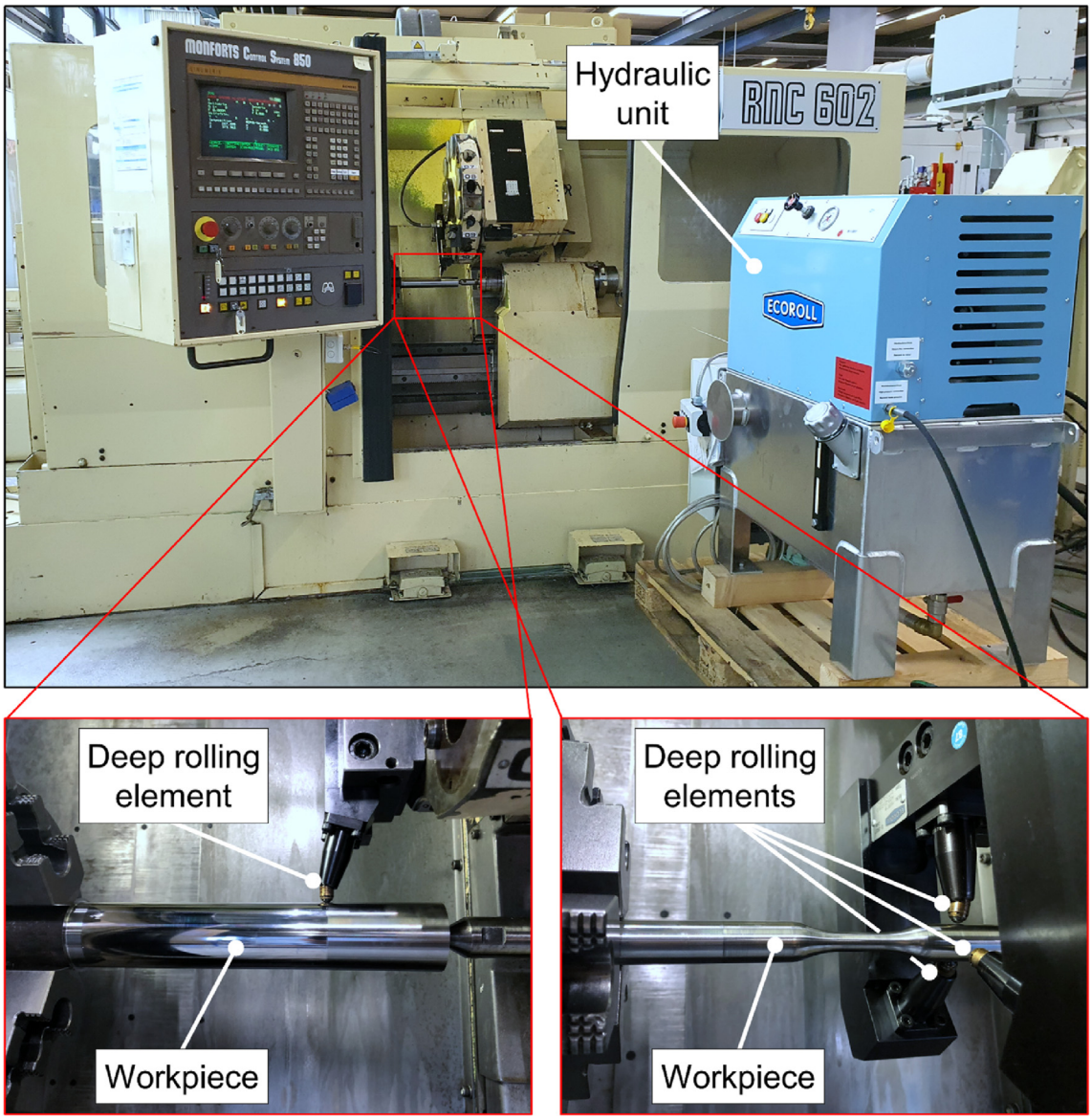

Fig. 2 – Experimental setup for deep rolling of the two types of specimens. The parameters employed for deep rolling are depicted in Table 4.

FracDim (Fraunhofer IKTS, Dresden, Germany). A multipurpose sensor was employed, consisting of a magnetic yoke, an induction coil and a magnetic field sensor. A detailed illustration of the sensor is presented in [9]. For all experiments magnetic field strength was set to Phi_{max} = 4.7 μVs. A magnetization frequency of f_{mag} = 60 Hz and a bandpass of f_{low} - f_{high} = 10–200 kHz were used. These parameters were chosen based on results of previous measurements of machined AISI 4140+QT [9,10]. Three repeated measurements were performed for each position of the specimen, to analyze the impact of the process stages on the residual stress state in the subsurface (deep rolling; deep rolling + 1st stage of microfinishing; deep rolling + 1st, 2nd stage of microfinishing; deep rolling + 1st, 2nd, 3rd stage of microfinishing). The micromagnetic parameter extracted from the magnetic hysteresis for the characterization of surface integrity was the Barkhausen envelope maximum M_{max} which occurs when the coercive field strength is applied.

3. Results and discussions

3.1. *Results of the topographic analysis*

The surface of the turned workpiece section (residual stress test specimen, type B) recorded with a confocal white-light microscope shows a process-typical topography (Fig. 5 a). Depending on the feed rate set for turning, the cutting edge shape of the indexable insert used becomes visible on the workpiece surface. These clearly visible tool-related roughness peaks are reflected in the increased surface parameters, which are shown in the box–plot diagram (Fig. 5 a). The

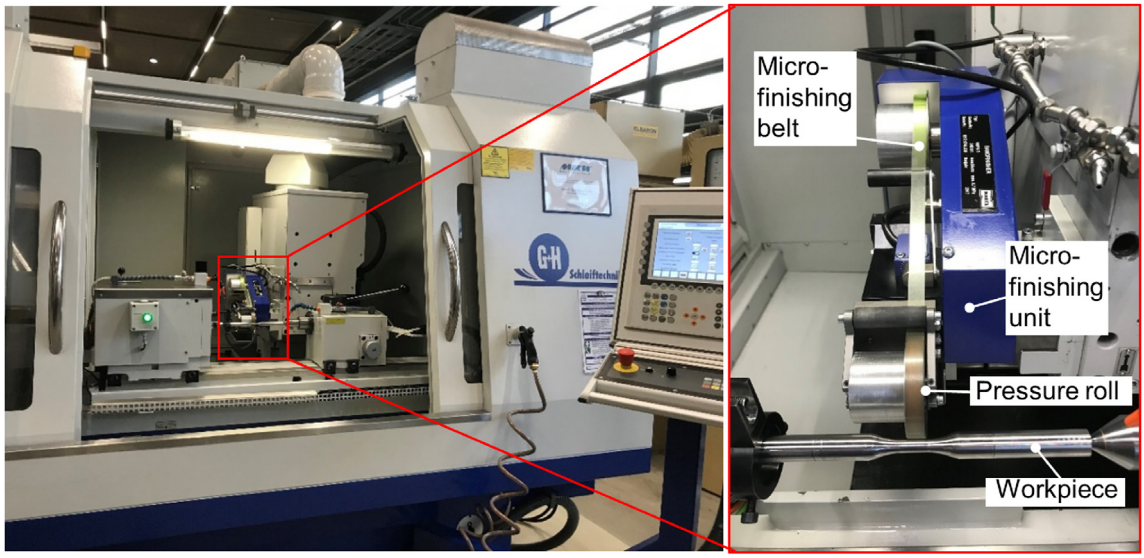

Fig. 3 – Experimental setup for microfinishing of the two types of specimens.

increased surface roughness (Rz = 9.21 μm) is primarily dominated by the comparatively high amount of peaks periodically protruding out of the profile, which is also evident in the increased Rpk value (Rpk = 4.63 μm). However, for a functional surface with increased contact ratio, this Rpk value should be considerably lower than the Rk value (Rk = 3.62 μm), which is also considered too high for a load-bearing surface. While a surface characterized by such topography is unsuitable for sliding processes, e.g. for cylinder tracks in engines or for rolling bearings, pronounced roughness peaks on the other hand are essential for a significant induction of compressive residual stresses resulting from deep rolling. The reason for the improvement of compressive residual stresses when deep rolling is the occurring internal material flow, the levelling of the roughness peaks with simultaneous lifting of the roughness valleys, and the associated work hardening of the material in the subsurface.

Considering the section deep rolled in a single pass (Fig. 5 b) and taking into account the respective box–plot diagram of the specimen type B deep rolled one time, before microfinishing shown in Fig. 5 b), it can already be assumed that significantly high compressive residual stresses were induced in the subsurface of the specimens. This correlation between the removal of roughness peaks and the induction of compressive residual stresses in deep rolling is well reported [20]. Even by a single deep rolling process, the pronounced roughness peaks were completely levelled and the roughness valleys were lifted as far as possible (Rpk ≈ Rvk). Due to the resulting distinct surface smoothing (Rz < 0.5 μm) and the associated high material flow, increased compressive residual stresses are expected. While in 3D-topography of the specimens deep rolled one time, partially existing inhomogeneities in the workpiece surface are visible, these seem to be sufficiently eliminated by deep rolling the specimens twice (Fig. 5 c). Even if the further reduction of the characteristic values with an additional deep rolling path is only slight, a corresponding effect can be seen. Thus, an increase in the homogeneity of the surface can be achieved by increasing the rolling processes. This clearly positive impairment, regarding the surface roughness, due to the double deep rolling process can be observed equally evident in the surface white-light image of the residual stress test specimen shown in Fig. 5 c).

The surfaces of the specimens have the process typical topography after microfinishing shown in the three-dimensional images in **Fig. 6**. Due to the low roughness values, the scale was adjusted in comparison to Fig. 5. In the first step of the microfinishing process (Fig. 6 a) a significant cross-grid topography is created. Therefore, the median of

Table 5 – Parameters used for microfinishing the two types of specimens.

Type	Process stage	Grain size d_K (μm)	Belt feed speed v_{fb} (mm•min^{-1})	Cutting time t_c (s)	Normal force F_n (N)	Surface pressure p_{FL} (N•mm^{-2})	Cutting speed v_c (m•min^{-1})	Oscillation frequency f_{os} (Hz)
Fatigue strength test (Type A)	1	30	100	20	80	1.5	20	11.2
	2	9	100	10	80	1.5	20	11.2
	3	3	100	10	80	1.5	20	11.2
Residual stress test (Type B)	1	30	100	20	140	1.5	20	11.2
	2	9	100	10	140	1.5	20	11.2
	3	3	100	10	140	1.5	20	11.2

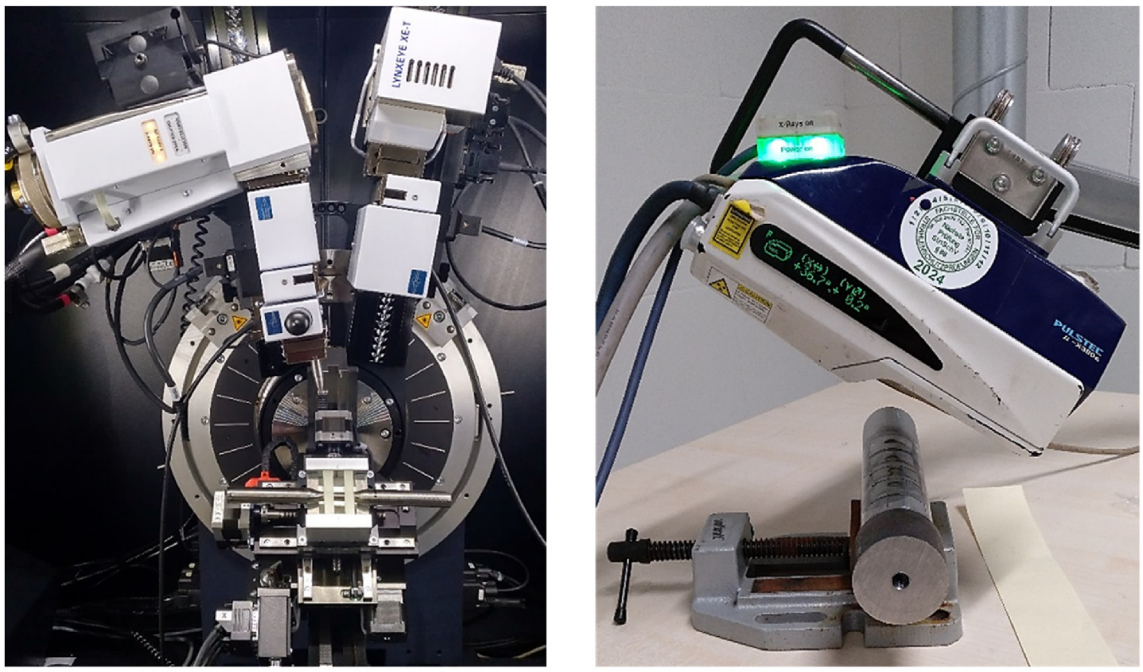

Fig. 4 – Setup for diffractometric analyses: (a) Bruker D8 Discover diffractometer, here shown as used for the analysis of specimens for fatigue tests (type A); (b) Pulstec μ-X360s, here shown as used for the analysis of residual stress test specimens (type B).

maximum height of the profile (Rz = 1.90 μm) increases compared to the deep rolled surfaces. The height of the peaks is characterized by the reduced peak height (Rpk) and the depth of the grooves is described by the reduced valley depth (Rvk). In the first microfinishing step the reduced peak height (Rpk = 0.32 μm) has a higher median than the reduced valley depth (Rvk = 0.26 μm). The next two stages in the microfinishing process are used to create a plateau structured topography and thus smoothen the surface.

Within the second and the third microfinishing stages the maximum height of the profile Rz is decreased to Rz = 0.19 μm after the third process stage. Due to the smaller grain size the reduced peak height Rpk is decreased. Compared to the reduced peak height the reduced valley depth is higher (Rpk < Rvk) after the second and the third stages of the microfinishing steps. It was possible to create a plateau structured topography, which is advantageous for tribological applications of components in most cases. Furthermore, Fig. 7 indicates that the surface roughness achieved by microfinishing is largely the same even for different input roughness. The different initial conditions before finishing are based on the variation of feed rate and number of passes during deep rolling.

The high scattering of the mean roughness depth values during deep rolling with low feed and two passes can be explained by these parameters. Due to the low feed, the individual rolling paths are very close together, so that overlapping of material or so-called bulges can occur. The double overrolling can additionally intensify this effect. During the subsequent finishing process, the finishing belt with a grain size of d_K = 30 μm gradually removes the surface so that the roughness peaks responsible for the high roughness can be removed. Only in the further process are new grooves introduced into the surface. The resulting surface quality of identical workpieces in microfinishing with a belt always depends on the quality of the microfinishing belt, grain size and grain application, assuming sufficient processing time and belt feed. For finer initial surfaces, the achievable surface finish is in principle reached more quickly without the result differing

Table 6 – Parameters for the diffractometric analysis of residual stresses. Values for Young's modulus and Poisson's ratio vary in precision, since the experiments were carried out by different laboratories.

System	Tube	Diameter of the collimator	Bragg angle	Current	Voltage	Young's modulus	Poisson's ratio
Bruker D8 Discover	Cr	0.3 mm	156°	40 mA	30 kV	220 GPa	0.28
Pulstec μ-X360s	Cr	0.3 mm/2.0 mm	156°	1.5 mA	30 kV	210 GPa	0.3

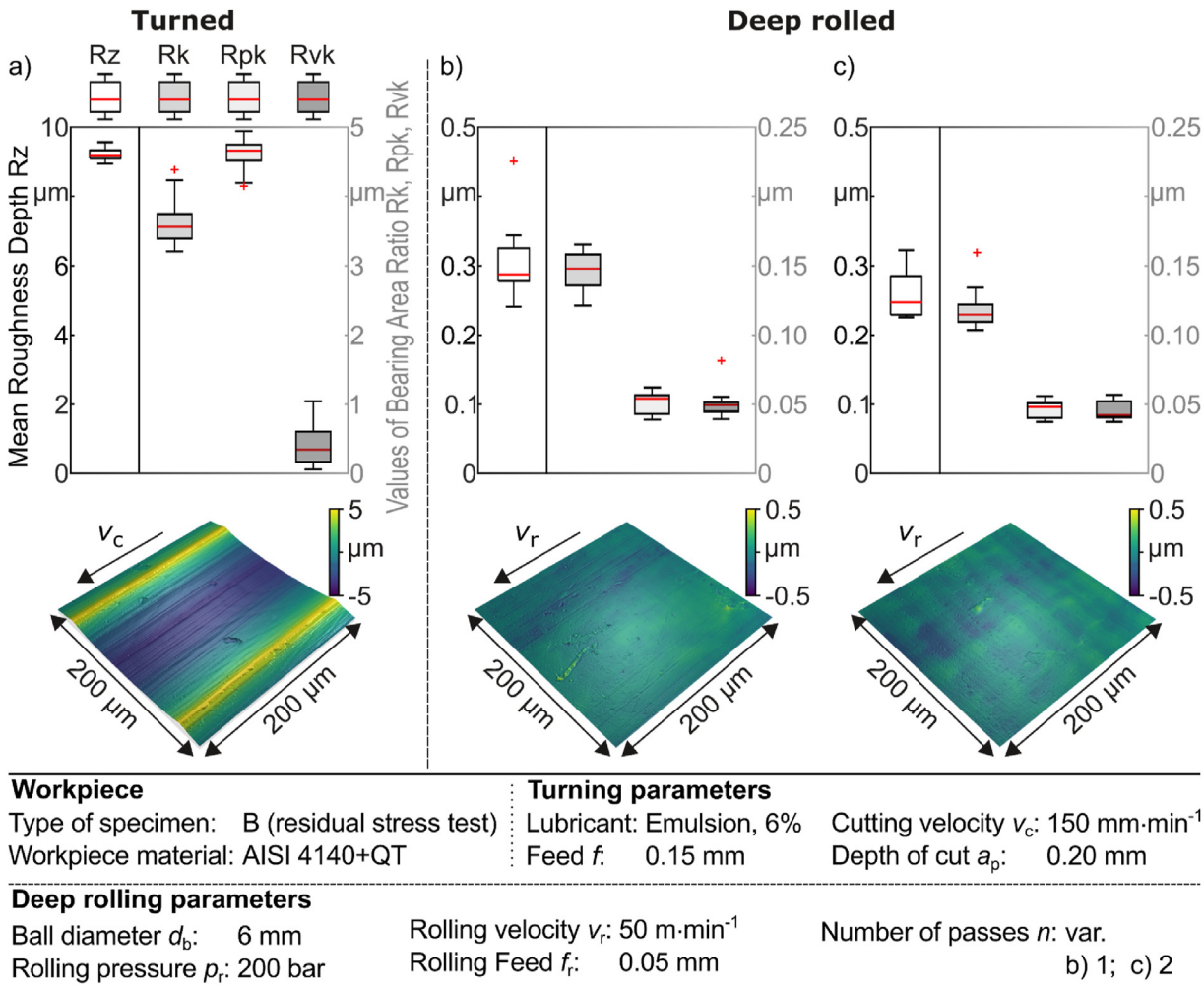

Fig. 5 – Topographies and surface parameters of a) Turned and b) and c) Deep-rolled specimens.

greatly. The final surface topography, which is then produced by the three-stage microfinishing process, is identical regardless of the different initial topographies.

Based on the low material removal it can be assumed, that only the topography and subsurface near zones are influenced by microfinishing and thus the process does not generate critical thermomechanical loads that can lead to damage in the subsurface layers. To support the hypothesis, the depth of material removal along the axis was recorded and evaluated. The maximum height of material removal l_m in a two-dimensional scale after all three microfinishing stages is shown in Fig. 8. The maximum height of material removal after all three microfinishing stages is approx. $l_m \approx 3–4$ µm.

Based on the process kinematics the material removal is not constant in axial direction. The tool oscillation with an amplitude of S = ±2 mm leads to lower material removal on the sides of the contact zone. This effect is clearly visible in Fig. 8.

3.2. *Results of the metallographic analysis*

The microstructure of subsurface area after deep rolling in cross-sections of residual stress test specimens (type B) is depicted in Fig. 9 and Fig. 10. The gradient layer (GL), aroused due to severe plastic deformation while deep rolling can be clearly distinguished from microstructure of base material (BM) based on size of carbides and their distribution. As an effect of severe plastic deformation, the size of grains as well as of carbides in the gradient layer is decreasing, leading to a microstructure with finely distributed carbides. The grain boundaries, well defined in the base material, become less visible in the gradient layer due to the small grain size. Owing to high shear stresses in the contact zone, the upper nano-structured surface layer (NSL) possesses very fine carbides with a size less than 100 nm, grain boundaries cannot be distinguished.

Figure 10 demonstrates the evolution of microstructure of the subsurface area during microfinishing. As it can be seen in Fig. 10, deep rolling ④ causes severe plastic deformation of the upper surface layer up to 5 µm deep, resulting in a gradient microstructure GL. The difference between 1 and 2 passes of deep rolling can be noticed in the width of the gradient layer of the subsurface. Two passes of deep rolling result in an almost twice as deep gradient layer with an almost amorphous microstructure of the nanostructured surface layer NSL. After the 1st stage of microfinishing ①, the upper subsurface layer NSL was removed, but the difference between 1 and 2 passes

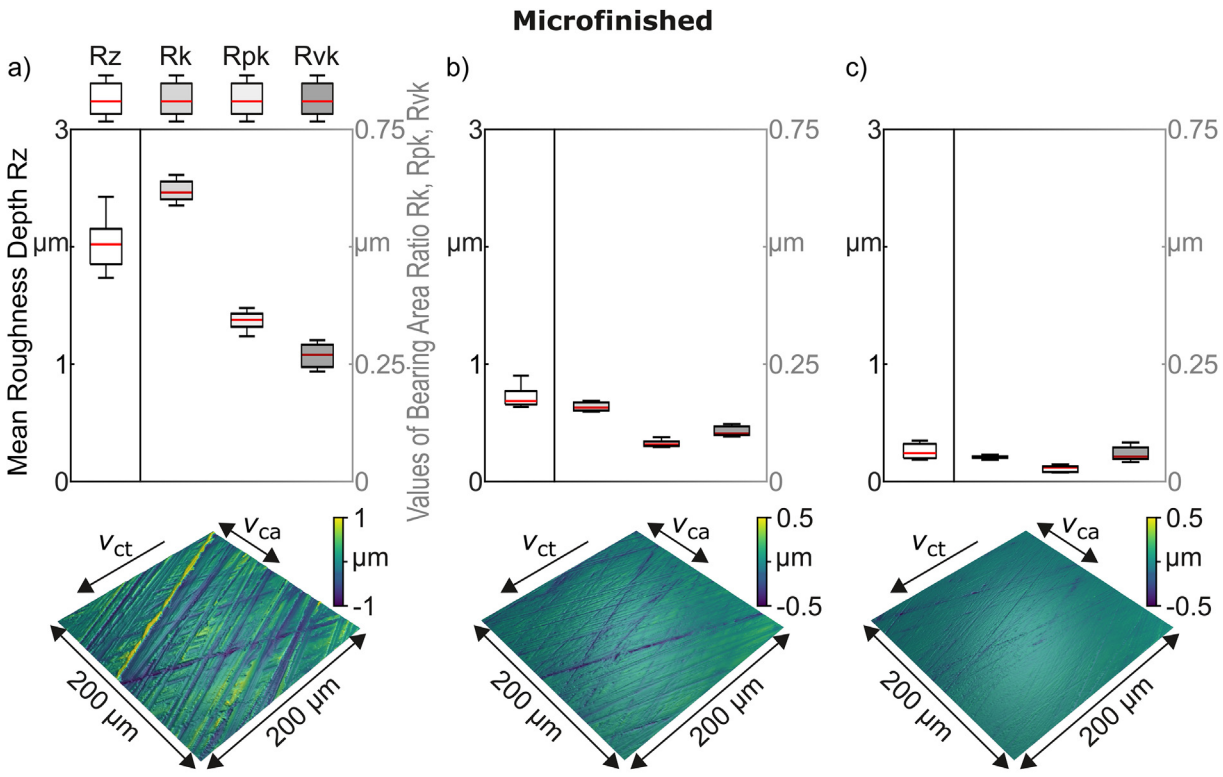

Workpiece		Deep roling parameters			
Type of specimen:	B (residual stress test)	Rolling velocity v_r:	50 m·min^{-1}	Rolling feed f_r:	0.05 mm
Workpiece material:	AISI 4140+QT	Ball diameter d_b:	6 mm	Number of passes n:	1
Initial state:	Turned & deep rolled	Rolling pressure p_r:	200 bar		

Microfinishing parameters					
Pressure roll hardness:	60° Shore A	Os. amplitude S:	±2 mm	Normal force F_n:	140 N
(Stage-)Grain size d_K:	a) 1. D30	Belt feed rate v_{fb}:	100 mm min^{-1}	Surface pressure p_{Fl}:	1.5 N·mm^{-2}
	b) 2. D9	Cutting time t_c:	a) 20s;	Tangential velocity v_t:	11.3 m·min^{-1}
	c) 3. D3		b, c) 10s	Os. frequency f_{Os}:	11.2 Hz
				Res. cutting velocity v_c:	12.7 m·min^{-1}

Fig. 6 – Topographies and surface parameters of microfinished specimens after a) One b) Two and c) Three microfinishing stages.

of deep rolling remains and can be estimated by the width of the gradient layer. This difference disappears after the 2nd stage of microfinishing ②, the width of the gradient layer is significantly reduced, the subsurface area has almost the same microstructure as the base material. After the 3rd stage of microfinishing ③ the gradient layer is completely removed for both types of deep rolling specimens.

3.3. *Results of the residual stress measurements*

3.3.1. *X-ray diffractometry*

Figure 11 displays the residual stresses close to the surface of specimens for fatigue tests (type A), evaluated by X-ray diffraction according to $\sin^2 \psi$ (Fig. 11a) and $\cos \alpha$ (Fig. 11b) methods. The error bars indicate the errors in the calculation of residual stresses, resulting from the mathematical algorithms employed. They can thus be considered the error of every single measurement and used to assess the quality of the data used for the calculation of residual stresses.

The turned specimens (Type A) were found to have tensile residual stresses in the subsurface in axial as well as tangential direction of up to approx. $\sigma_{Axial} \approx 450$ MPa and $\sigma_{Tangential} \approx 350$ MPa. The mechanisms that cause the formation of residual stresses in turning are complex and still not fully understood [1]. However, the feed rate and the cutting edge radius have been identified as the main parameters that pose an influence on residual stresses in the subsurface of turned specimens. In general, tensile residual stresses are common for turned surfaces, particularly when using relatively high feed rates, due to elevated thermomechanical loads impinged on the workpieces during turning [1].

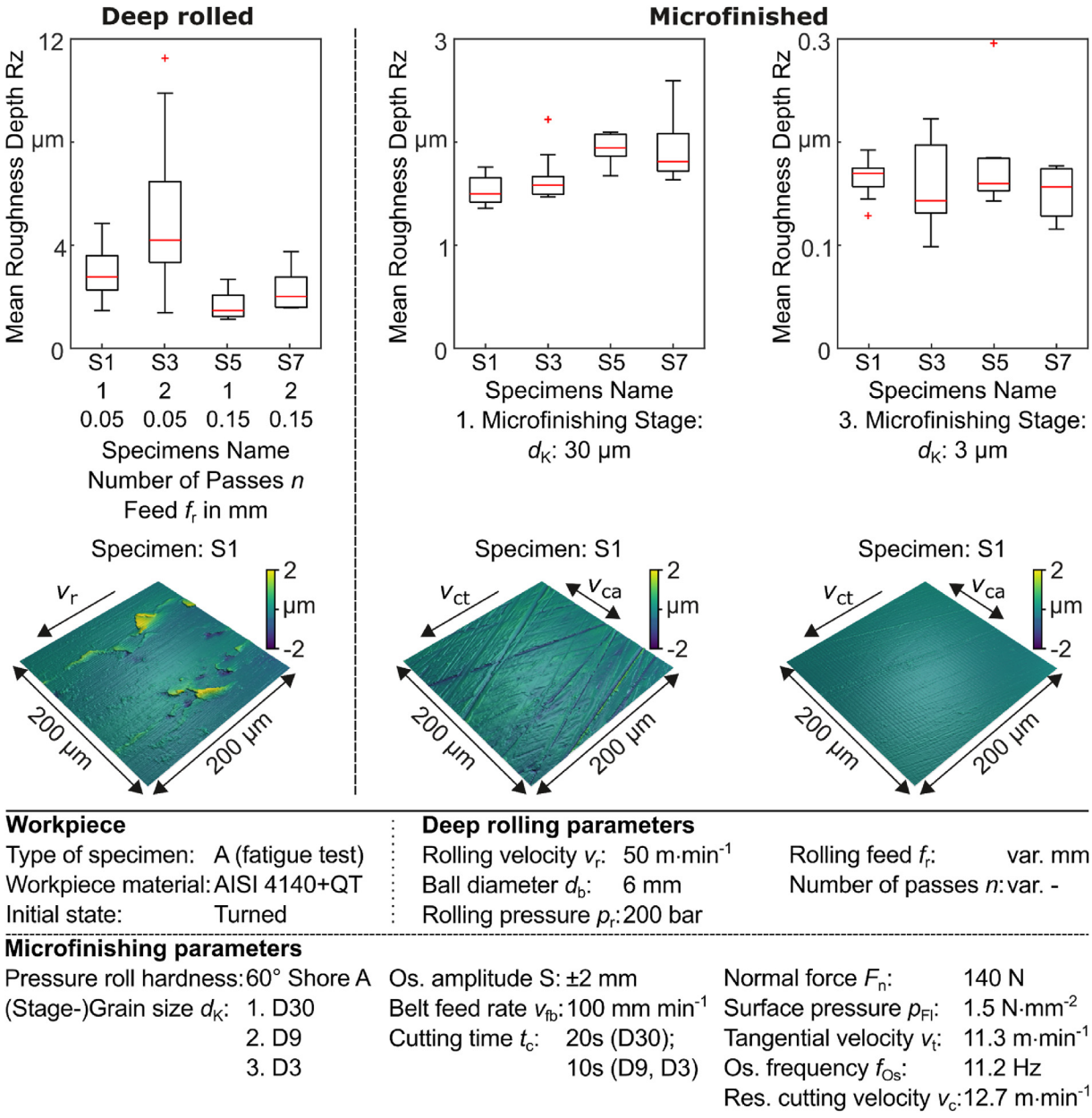

Fig. 7 – Topographies and mean roughness values Rz of a) Deep rolled specimen and after the b) First and c) Third microfinishing stage.

Deep rolling was found to induce significant compressive residual stresses of approx. $\sigma_{Axial} \approx -750$ MPa and -1100 MPa in axial direction. In tangential direction, the intensity of the residual stresses is lower. Compressive residual stresses with an intensity of up to approx. $\sigma_{Tangential} \approx -200$ MPa to -500 MPa were measured. This corresponds well to the findings of Beghini et al.: They found that residual stresses in axial direction can exceed residual stresses in tangential direction by two times after deep rolling and identify the preferential flow of material in feed direction and the curvature of the tool as major reasons for this anisotropy [20]. The number of rolling passes and the feed rate, which are known to be main parameters during deep rolling do not show a significant impact on the residual stress state [24]. This agrees to the findings presented in [16]. After being subjected to a microfinishing process, the deep rolled specimens show compressive residual stress in axial direction with an intensity of up to approx. $\sigma_{Axial} = -600$ MPa. Tangential residual stresses are approx. at the same level as right after deep rolling with an intensity of up to approx. $\sigma_{Tangential} \approx -450$ MPa. For all surface states investigated both diffractometric approaches showed relatively good agreement (Fig. 11).

Figure 12 displays a comparison between the residual stresses measured by Bruker D8 Discover ($\sin^2 \psi$-method) and Pulstec µ-X360s (cos α-method). Reasons for the slight differences in the intensity of residual stresses between the two methods might be found in the alignment of the specimens during the measurements. In addition to this, differences in

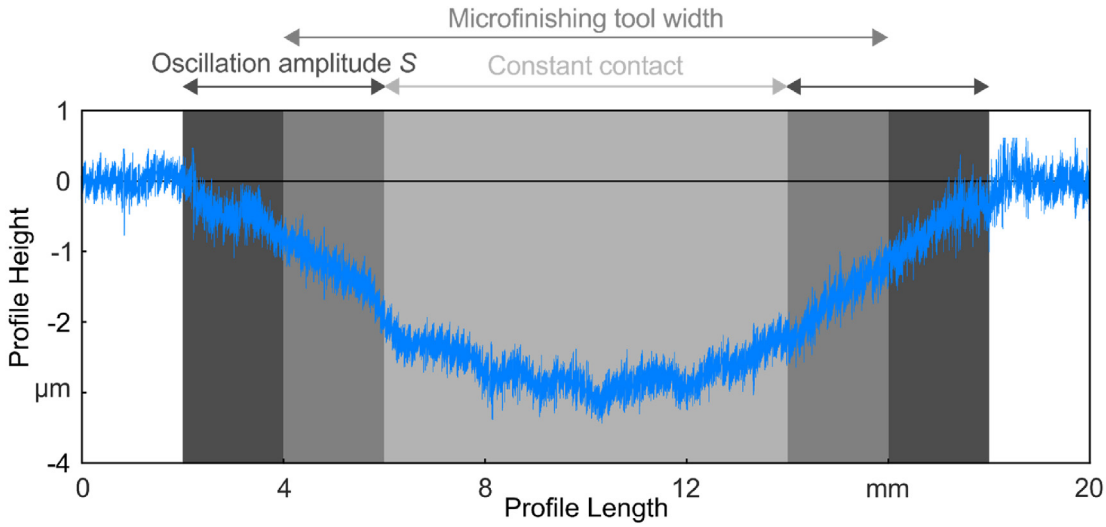

Workpiece		Deep rolling parameters			
Type of specimen:	B (residual stress test)	Rolling velocity v_r:	50 m·min^{-1}	Rolling feed f_r:	0.05 mm
Workpiece material:	AISI 4140+QT	Ball diameter d_b:	6 mm	Number of passes n:	1
Initial state:	Turned & deep rolled	Rolling pressure p_r:	200 bar		

Microfinishing parameters					
Pressure roll hardness:	60° Shore A	Os. amplitude S:	±2 mm	Normal force F_n:	140 N
(Stage-)Grain size d_K:	D30, D9, D3	Belt feed rate v_{fb}:	100 mm min^{-1}	Surface pressure p_{FI}:	1.5 N·mm^{-2}
		Cutting time t_c:	20s, 10s, 10s	Tangential velocity v_t:	11.3 m·min^{-1}
				Os. frequency f_{Os}:	11.2 Hz
				Res. cutting velocity v_c:	12.7 m·min^{-1}

Fig. 8 – Exemplarily contour depicting the resulting material removal by means of the three stage microfinishing process.

the evaluation algorithms used for calculating the residual stresses based on the elastic lattice strains measured might be accountable for the observed differences. This includes the precision of the material properties Young's modulus and Poisson's ratio used by the devices for the calculation of stresses, which also could account for remaining differences ($E_{\mu\text{-}X360s} = 210$ GPa; $E_{D8} = 220$ GPa; $\nu_{\mu\text{-}X360s} = 0.3$; $\nu_{D8} = 0.28$). The results correspond to the findings of Ramirez-Rico et al.

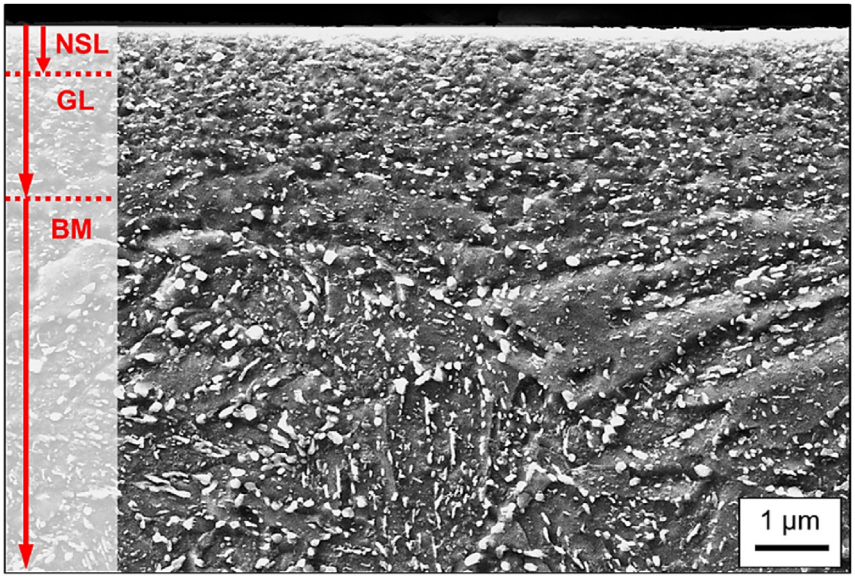

Fig. 9 – Microstructure of the subsurface area after deep rolling in cross-sections of residual stress test specimens (type B). BM: base material; GL: gradient layer; NSL: nanostructured surface layer.

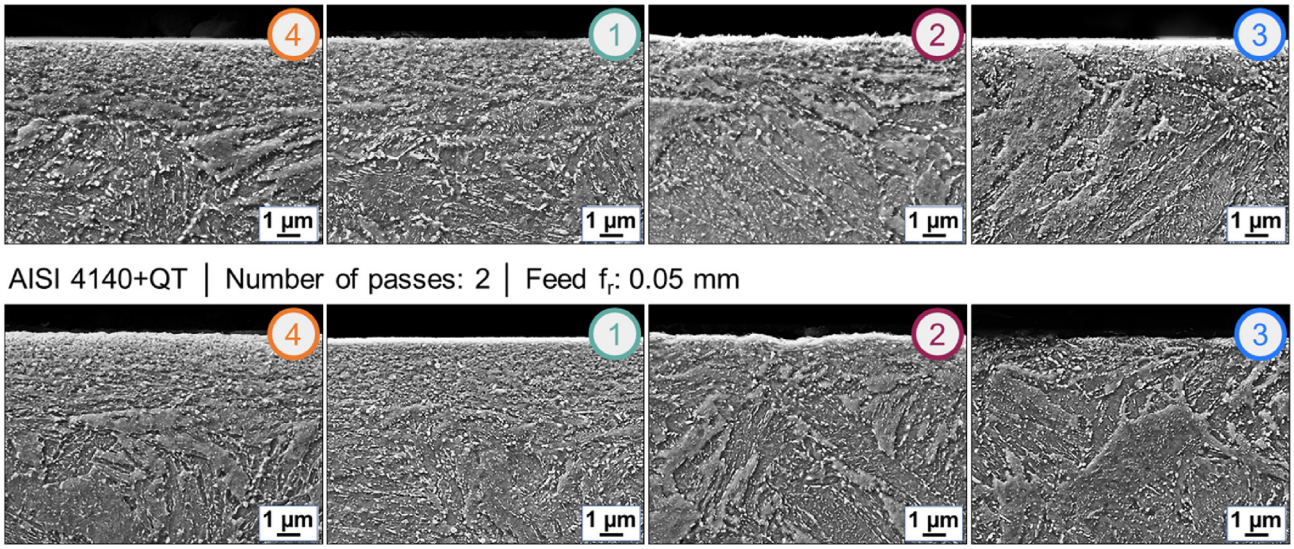

Fig. 10 – Microstructure of the surface layer in cross-sections of residual stress test specimens (Type B). ①: deep rolling +1st stage of microfinishing; ②: deep rolling +1st, 2nd stage of microfinishing; ③: deep rolling +1st, 2nd, 3rd stage of microfinishing; ④: deep rolling - as shown in Fig. 1.

who provided evidence that cos α- and $\sin^2 \psi$-methods deliver similar results, given that a number of different criteria are met [40].

Whereas for most cutting processes like turning the variation of residual stresses inside a specimen is well analyzed, there are only limited studies that consider this matter for deep rolled specimens [20,41]. For this reason and for an enhanced statistical basis of the analysis, a deep rolled and microfinished specimen of type A ($f = 0.15$ mm; $n = 2$) was analyzed at three different positions (MP1-MP3) in axial as well as tangential direction, to analyze circumferential variation of residual stresses (Fig. 13). Three repetitive measurements were performed at each position (e.g. 1.1–1.3). Between each of the measurements, the specimen was taken out and realigned. It was found, that there is relatively little circumferential variation in the intensity of compressive residual stresses and that there is very good repeatability of the measurements: Axial residual stresses are in the range of $\sigma_{Axial} = -613$ to -749 MPa, in tangential direction in the range of approx. $\sigma_{Tangential} = -340$ to -421 MPa.

Figure 14 depicts depth profiles of the residual stresses in the specimens for residual stress tests (type B). Just like for the specimens of type A, it is found that close to the surface, stresses in axial direction significantly exceed stresses in tangential direction. The reason for this discrepancy between the stress components might be found in the shape of the tool

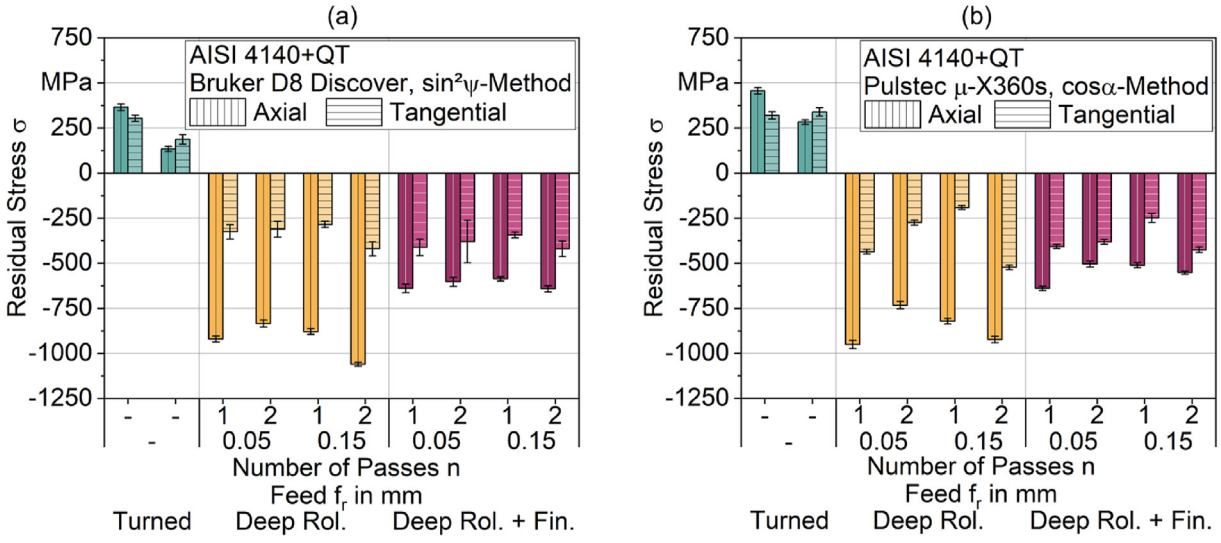

Fig. 11 – Residual stresses in axial and tangential direction for turned, deep rolled and deep rolled and microfinished specimens for fatigue tests (type A) measured by Bruker D8 Discover ($\sin^2 \psi$-method) and Pulstec µ-X360s (cos α-method).

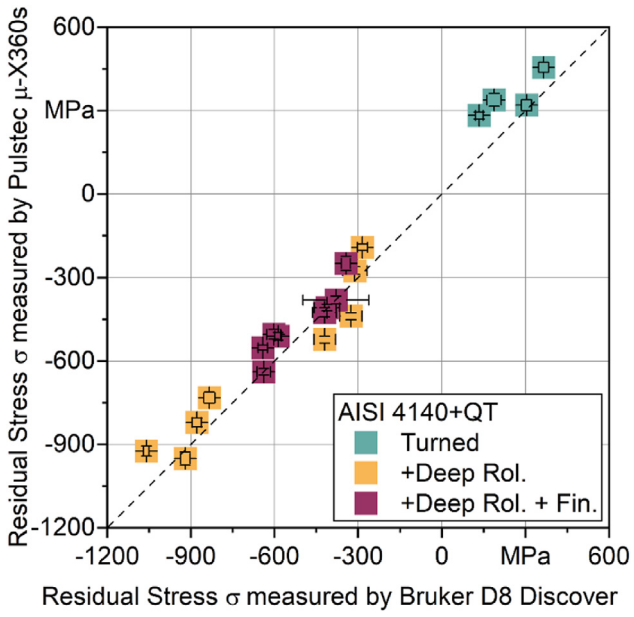

Fig. 12 – Comparison between the residual stresses in specimens for fatigue tests (type A) measured by Bruker D8 Discover ($\sin^2\psi$-method) and Pulstec μ-X360s (cos α-method).

and the preferential flow of material in feed direction during deep rolling, as pointed out in [20]. In the deep rolled area (4), a significant drop in the intensity of compressive residual stresses in axial direction right below the surface can be observed. This is typical for deep rolled specimens when using relatively low deep rolling forces, as with high deep rolling forces the maximum intensity is usually shifted to deeper subsurface layers [14,20]. Based on these observations, the conclusion can be drawn that the material-specific limit, as previously explained in the introduction, is not reached using the setup employed and the deep rolling pressure of p_r = 200 bar. Close to the surface of the specimen, residual stresses of $\sigma_{Axial} \approx -800$ MPa were measured for the deep rolled areas and $\sigma_{Axial} \approx -500$ MPa for the areas that were subjected to deep rolling and microfinishing. This corresponds very well to the analysis of the fatigue test specimens (type A) (Fig. 11). In contrast to the depth profile of the area subjected to deep rolling only, all areas subjected to microfinishing after deep rolling (1–3) show a slight increase in the intensity of compressive residual stresses in axial direction until a depth of h = 100 μm. After this point their intensity decreases as well. The reason for this shape of depth profiles caused by deep rolling and subsequent microfinishing might be found in various overlapping effects of microfinishing. On the one hand it can be assumed that the removal of the layer with the highest compressive residual stresses during microfinishing might account for the lower intensity of residual stresses after microfinishing. On the other hand, the thermomechanical loads during microfinishing might cause a slight alteration of residual stresses in axial direction. No significant difference in residual stresses caused by the different microfinishing process stages was identified. Thus, the conclusion can be drawn, that the residual stress state in microfinishing is mainly influenced by the first process stage, which is the process stage in which most of the material is removed in microfinishing.

In tangential direction there is little variation in residual stresses for all specimens investigated and relatively small differences between the areas subjected to deep rolling and deep rolling followed by microfinishing was observed. Elevated compressive residual stresses with an intensity of $|\sigma| > 300$ MPa were still measured in a depth of h = 300 μm (Fig. 14). Based on these observations, it can be concluded that microfinishing following deep rolling mostly has an influence on the axial component of the residual stress state. No significant difference was found between the specimen subjected to one pass of the tool and the specimen subjected to two passes. This is in good agreement to the findings in [16]

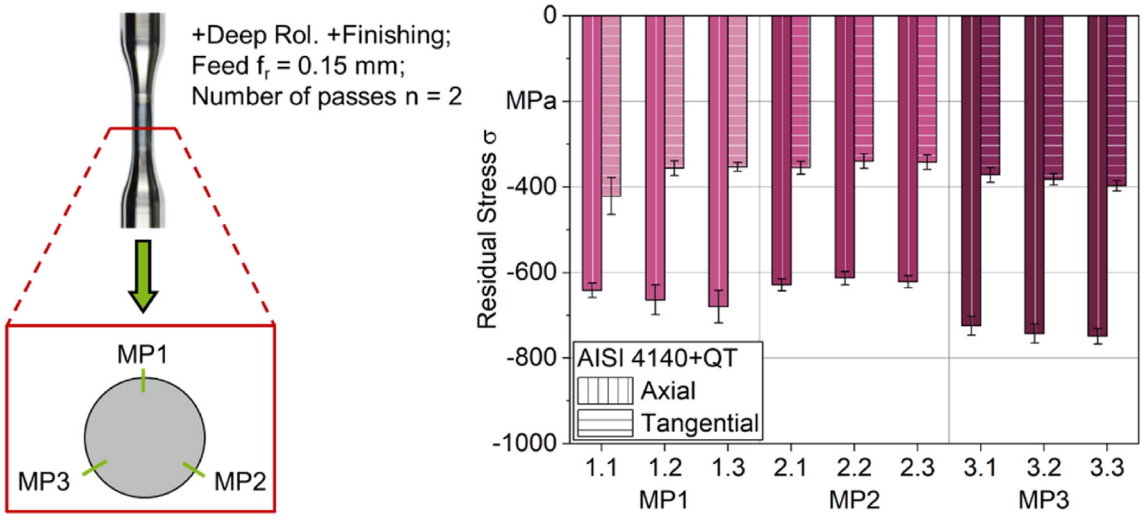

Fig. 13 – Residual stresses at three different positions (MP1; MP2; MP3) around the circumference of specimens for fatigue tests (type A) in axial and tangential direction measured with Bruker D8 Discover ($\sin^2\psi$-method).

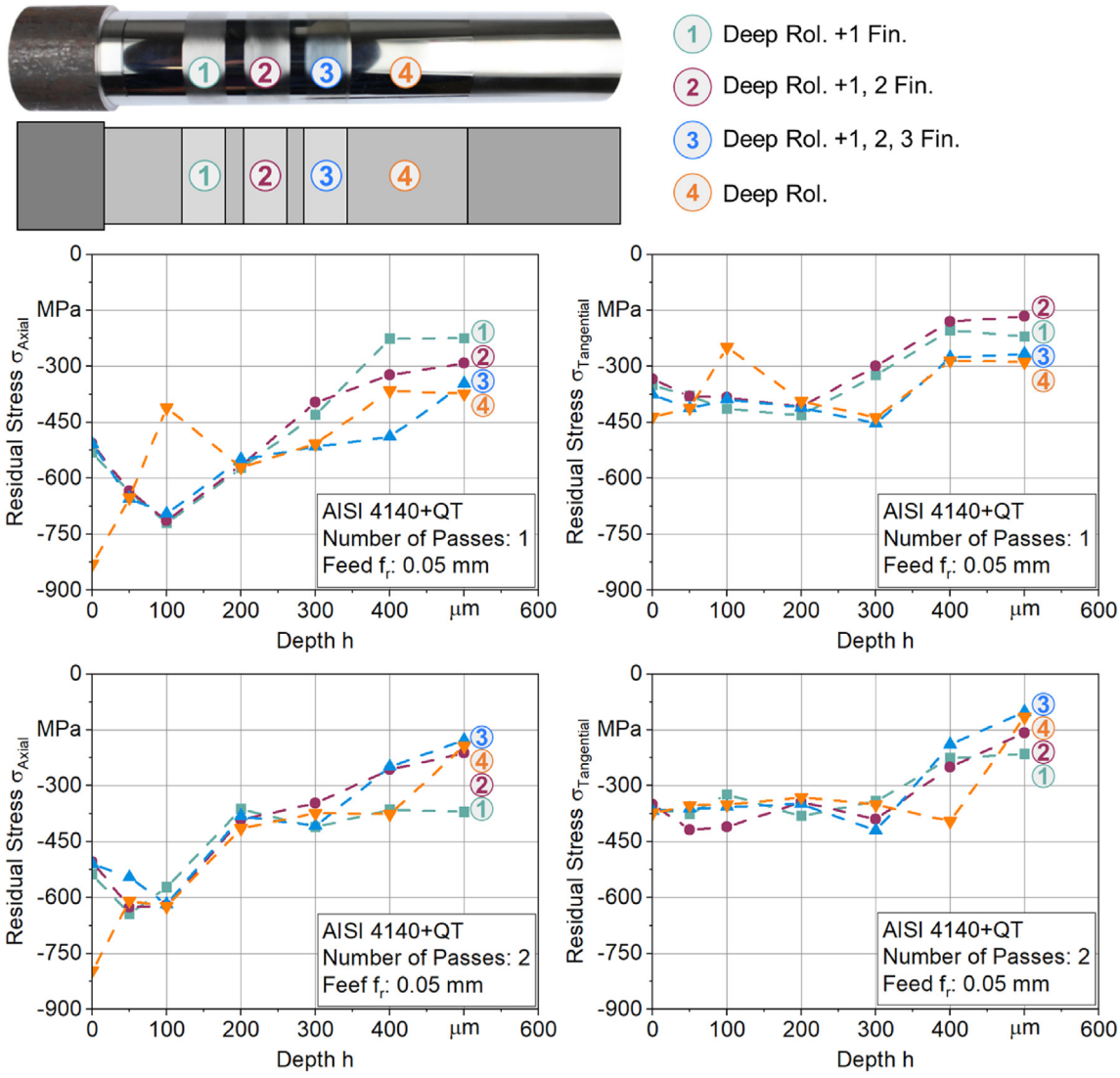

Fig. 14 – Residual stresses for various finishing states and different deep rolling parameters in axial and tangential direction in specimens for residual stress tests (type B), assessed by cos α-method.

and indicates that one deep rolling pass can be sufficient for inducing high compressive residual stresses.

3.3.2. *Micromagnetic methods*

Magnetic Barkhausen noise analysis is used as a holistic approach for a time-efficient and non-destructive characterization of various aspects of surface integrity like microstructure and residual stresses. Using the micromagnetic investigations it was found, that surface integrity in deep rolled and microfinished specimens varied from surface integrity of specimens, which were only subjected to deep rolling. Figure 15 depicts the maximum MBN amplitude M_{max} for different surface states along with the residual stresses detected in axial and tangential direction. Specimens subjected only to deep rolling show significantly lower M_{max} values. The reason for this might be found in the higher compressive residual stresses in axial direction in the subsurface of the deep rolled material and in the reduction of the thickness of the gradient layer during finishing. Between the various finishing steps, no significant difference was found in the MBN amplitudes. This corresponds well to the findings of the two approaches in X-ray diffractometry which showed that there is no significant difference in residual stresses between the various microfinishing process stages. The specimen subjected to two passes of the deep rolling tool, exhibits similar residual stresses as the specimen subjected to only one pass. However, the MBN amplitudes of the specimen subjected to two passes are significantly lower than the amplitudes detected for one pass of the deep rolling tool. The explanation can be found in the differences in microstructure between the two specimens (Fig. 10). As it was outlined in 3.2., the specimen subjected to two passes of the deep rolling tool had a gradient layer with an almost amorphous microstructure on the surface that was approx. twice as deep as the layer found in the specimen subjected to only one pass of the deep rolling tool. This variation of microstructure caused by the alteration of the deep rolling process results in the difference in magnetic Barkhausen noise amplitude.

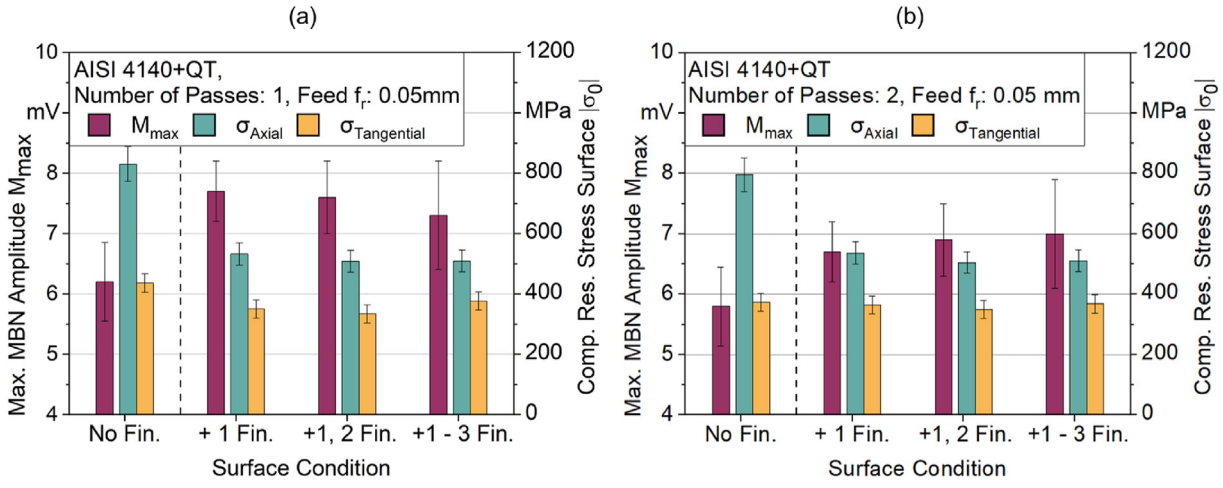

Fig. 15 – Magnetic Barkhausen noise and residual stresses for deep rolled (No Fin.) and deep rolled and microfinished (+ X Fin.) specimens for residual stress tests (type B). Error bars indicate the standard deviation for M_{max} and the calculated statistical error for σ_0. X refers to the microfinishing process stages, the specimen was subjected to.

Based on the results of micromagnetic measurements, X-ray diffractometry and metallographic analyses, it can be concluded that the analysis of MBN can be used as an additional tool for a holistic characterization of surface integrity resulting from deep rolling and subsequent microfinishing. However, it couldn't be clearly and unambiguously distinguished between the effects of microstructure and residual stress state on MBN by M_{max}. In the future, further parameters, like coercivity will be analyzed for an enhanced interpretation of micromagnetic parameters. This might allow identifying further correlations between mechanical and micromagnetic properties.

4. Conclusions and outlook

High compressive residual stresses induced in the subsurface by means of the deep rolling process were characterized using $\sin^2\psi$- and cos α-methods in X-ray diffractometry. The intensity of residual stresses close to the surface in axial direction was in the range of $\sigma_{Axial} \approx -750$ to -1100 MPa. In the tangential direction compressive stresses were measured in the range of $\sigma_{Tantential} \approx -200$ to -500 MPa. The number of passes of the deep rolling tool and the feed f_r did not significantly affect the residual stresses at the surface of the specimens. The impact of deep rolling reached up to depth of $h > 500$ μm.

Microfinishing following deep rolling showed a moderate impact on the residual stress state of the specimens. Specimens subjected to microfinishing after deep rolling showed elevated compressive residual stresses at the surface with an intensity of up to $\sigma_{Axial} \approx -750$ MPa in axial direction and up to $\sigma_{Tantential} \approx -450$ MPa in tangential direction. The different finishing process stages, did not affect the residual stresses in the subsurface of the specimens due to low thermomechanical loads during microfinishing. It was found that the combination of deep rolling and microfinishing leads to favorable properties, suitable for functional components in tribological applications. A surface with an adapted plateau structure could be created by microfinishing while maintaining relatively high compressive residual stress of up to $\sigma < -300$ MPa up to a depth of $h = 300$ μm.

The results of the two approaches in X-ray diffractometry showed very good agreement. Thus, for the specimens investigated X-ray diffractometry according to the cos α-method proved to be a time-efficient and reliable alternative for the $\sin^2\psi$-measurements, since cos α-method requires less complex instrumentation and less profound knowledge. In addition to this, measurements according to cos α-method can be performed in just a fraction of the time needed for $\sin^2\psi$-method ($t \approx 2.7$ min for cos α-method compared to $t \approx 220$ min for $\sin^2\psi$-method).

Metallographic analysis revealed that deep rolling leads to severe plastic deformation in the subsurface resulting in a complex gradient microstructure. The thickness of the gradient layer induced by two passes of the deep rolling tool was found to be almost twice the thickness of the layer caused by one pass of the deep rolling tool. The upper highly deformed surface layer is completely removed by microfinishing, equalizing the stress distribution on the upper subsurface without any negative impact on the high compressive residual stresses in depth of $h > 50$ μm.

Magnetic Barkhausen noise analysis proved to be well applicable for the holistic characterization of surface integrity resulting from deep rolling and microfinishing. Specimens possessing high compressive residual stresses and a thick layer with a gradient microstructure generally showed significantly lower magnetic Barkhausen noise amplitudes M_{max}. To separate the effects of microstructure and residual stresses on the micromagnetic properties, further investigations are required. In future studies, additional micromagnetic parameters like the coercive field strength will be considered with the aim of differentiating between the effects of microstructure and residual stresses on the micromagnetic properties. These efforts will aim towards the mechanism-oriented application of MBN for the fast and reliable assessment of residual stresses in deep rolled and microfinished surfaces. With respect to the production of tailored surfaces with a suitable combination of topography and subsurface, further possibilities will result from the process and analysis methodology to be developed.

5. Data availability

The raw/processed data required to reproduce these findings cannot be shared at this time as the data also forms part of an ongoing study.

Credit author statement

Simon Strodick: Investigation, Writing - original draft, Visualization.

Florian Vogel: Investigation, Writing - original draft, Visualization.

Marie Denstorf: Investigation, Writing - original draft, Visualization.

Meik Tilger: Writing - original draft, Visualization.

Monika Kipp: Writing - review & editing.

Nikolas Baak: Writing - review & editing.

Dimitri Kukui: Investigation.

Dirk Biermann: Supervision, Conceptualization, Writing - review & editing.

Marina Macias Barrientos: Supervision, Conceptualization, Writing - original draft, Visualization.

Frank Walther: Supervision, Conceptualization, Writing - review & editing.

Declaration of Competing Interest

The authors declare that they have no known competing financial interests or personal relationships that could have appeared to influence the work reported in this paper.

Acknowledgements

The authors thank the German Research Foundation (Deutsche Forschungsgemeinschaft, DFG) and the Ministry of Culture and Science of North Rhine-Westphalia (Ministerium für Kultur und Wissenschaft des Landes Nordrhein-Westfalen, MKW NRW) for their financial support within the Major Research Instrumentation Program for the X-ray diffractometer Bruker D8 Discover (XRD, DFG project no. 383863415) and focused ion beam scanning electron microscope Zeiss XB550 L (FIB-SEM, DFG project no. 386509496). The authors acknowledge financial support by the German Research Foundation and TU Dortmund University within the funding programme Open Access Costs (Open Access Publication Funding, DFG project no. 491021492).

REFERENCES

[1] Capello E. Residual stresses in turning Part I: influence of process parameters. J Mater Process Technol 2005;160(2):221–8.

[2] Fitzpatrick M, Fry A, Holdway P, Kandil F, Shackleton J, Suominen L. Determination of residual stresses by X-ray diffraction. Measurement good practice guide. Natl Phys Lab 2005;52:1–78.

[3] Delbergue D, Texier D, Lévesque M, Bocher P. Comparison of two X-ray residual stress measurement methods: $\sin^2\psi$ and $\cos\alpha$, through the determination of a martensitic steel X-Ray elastic constant. Mater Res Proc 2017:55–60.

[4] Tanaka K. The cosα method for X-ray residual stress measurement using two-dimensional detector. Mechanical Engineering Reviews 2019;6(1):1–15.

[5] Nielsen S, Wolf A, Poulsen H, Ohler M, Lienert U, Owen R. A conical slit for three-dimensional XRD mapping. J Synchrotron Radiat 2000;7(2):103–9.

[6] Marciszko M, Baczmański A, Klaus M, Genzel C, Oponowicz A, Wroński S, et al. A multireflection and multiwavelength residual stress determination method using energy dispersive diffraction. J Appl Crystallogr 2018;51(3):732–45.

[7] Woo W, Feng Z, Wang X, David S. Neutron diffraction measurements of residual stresses in friction stir welding: a review. Sci Technol Weld Join 2011;16(1):23–32.

[8] Reimers W. Analysis of residual stress states using diffraction methods. Acta Phys Pol, A 1999;96(2):229–38.

[9] Baak N, Hajavifard R, Lücker L, Rozo Vasquez J, Strodick S, Teschke M, et al. Micromagnetic approaches for microstructure analysis and capability assessment. Mater Char 2021;178:1–14. 111189.

[10] Strodick S, Berteld K, Schmidt R, Biermann D, Zabel A, Walther F. Influence of cutting parameters on the formation of white etching layers in BTA deep hole drilling. TM - Tech Mess 2020;11:674–82.

[11] Karpuschewski B, Bleicher O, Beutner M. Surface integrity inspection on gears using Barkhausen noise analysis. Proc Eng 2011;19:162–71.

[12] Baak N, Garlich M, Schmiedt A, Bambach M, Walther F. Characterization of residual stresses in austenitic disc springs induced by martensite formation during incremental forming using micromagnetic methods. Mater Test 2017;59(4):309–14.

[13] Jiles D. The effect of stress on magnetic Barkhausen activity in ferromagnetic steels. IEEE Trans Magn 1989;25(5):3455–7.

[14] Cherif A, Hochbein H, Zinn W, Scholtes B. Increase of fatigue strength and lifetime by deep rolling at elevated temperature of notched specimens made of steel SAE 4140. HTM J Heat Treatment Mater 2011;66(6):342–8.

[15] Denkena B, Grove T, Breidenstein B, Abrão A, Meyer K. Correlation between process load and deep rolling induced residual stress profiles. Proc CIRP 2018;78:161–5.

[16] Kämmler J, Wielki N, Meyer D. Surface integrity after internal load oriented multistage contact deep rolling. Proc CIRP 2018;71:490–5.

[17] Reggiani B, Olmi G. Experimental investigation on the effect of shot peening and deep rolling on the Fatigue response of high strength fasteners. Metals 2019;9(10):1093.

[18] Muñoz-Cubillos J, Coronado J, Rodríguez S. Deep rolling effect on fatigue behavior of austenitic stainless steels. Int J Fatig 2017;95:120–31.

[19] Zhang L, Lei L, Zeng P. Investigation of the influence of deep rolling on the thermal fatigue cracking for AISI H13 steel. Appl Mech Mater 2013;457–458:127–30.

[20] Beghini M, Bertini L, Monelli B, Santus C, Bandini M. Experimental parameter sensitivity analysis of residual stresses induced by deep rolling on 7075-T6 aluminium alloy. Surf Coating Technol 2014;254:175–86.

[21] Torres M. An evaluation of shot peening, residual stress and stress relaxation on the fatigue life of AISI 4340 steel. Int J Fatig 2002;24(8):877–86.

[22] Meyer D, Kämmler J. Surface integrity of AISI 4140 after deep rolling with varied external and internal loads. Proc CIRP 2016;45:363–6.

[23] Trauth D, Klocke F, Mattfeld P, Klink A. Time-efficient prediction of the surface layer state after deep rolling using similarity mechanics approach. Proc CIRP 2013;9:29–34.
[24] Abrão A, Denkena B, Köhler J, Breidenstein B, Mörke T. The influence of deep rolling on the surface integrity of AISI 1060 high carbon steel. Procedia CIRP 2014;13:31–6.
[25] Prabhu P, Prabhu D, Sharma S, Kulkarni S. Surface properties and corrosion behavior of turn-assisted deep-cold-rolled AISI 4140 steel. J Mater Eng Perform 2020;29(9):5871–85.
[26] Hashimoto F, Yamaguchi H, Krajnik P, Wegener K, Chaudhari R, Hoffmeister H-W, et al. Abrasive fine-finishing technology. CIRP Ann - Manuf Technol 2016;65(2):597–620.
[27] Goeke S. Oberflächenstrukturierung tribologisch beanspruchter Funktionsflächen durch Microfinishen (Surface structuring of tribologically stressed functional surfaces by microfinishing). PhD Thesis. TU Dortmund University; 2016.
[28] Schibisch D, Friedrich U. Feinste Oberflächen für höchste Präzision (Superfinish technology - finest surfaces for highest precision). Verlag Moderne Industrie; 2001.
[29] Goeke S, Biermann D, Stickel D, Stemmer P, Fischer A, Geenen K, et al. Enhancing the surface integrity of tribologically stressed contacting surfaces by an adjusted surface topography. Proc CIRP 2014;13:214–8.
[30] Khellouki A, Rech J, Zahouani H. Micro-scale investigation on belt finishing cutting mechanisms by scratch tests. Wear 2013;308(1–2):17–28.
[31] Martin K, Yegenoglu K. HSG-Technologie: handbuch zur praktischen Anwendung (HSG Technology: practical Application Manual. In: German), guehring automation GmbH: stetten a.k.M.-Frohnstetten; 1992.
[32] Martin K. Der Werkstoffabtragvorgang beim Feinbearbeitungsverfahren Honen (The material removal process in the fine machining process honing). Maschinenmarkt 1976;60:1074–8.
[33] Tilger M, Siebrecht T, Biermann D. Fundamental investigations of honing processes related to the material removal mechanisms. Proceedings of the 2017;7:121–8. WGP-Jahreskongress.
[34] Gahr K-H. Wear by hard particles. Tribol Int 1998;31(10):587–96.
[35] Biermann D, Abrahams H, Goeke S. Optimization of guide pads for the BTA deep hole drilling of high alloyed steels by microfinishing. J Inst Eng Prod 2014;8(1–2):33–40.
[36] Biermann D, Kansteiner M, Hess S, Joliet R. Mikrofinishen mit MMS oder Druckluftkühlung (Microfinishing with MQL or compressed air cooling). VDI-Z Integrierte Produktion 2014;156(7/8):57–9.
[37] Tilger M, Biermann D, Abdulgader M, Tillmann W. The effect of machined surface conditioning on the coating interface of high velocity oxygen fuel (HVOF) sprayed coating. J Manuf Mater Process 2019;3(79):1–17.
[38] Biermann D, Wiederkehr P, Kansteiner M, Tilger M. Einfluss der Andrückrollenhärte beim Microfinishen. Analyse der Kontaktbedingungen und der erzielten Oberflächenrauheiten (Influence of the pressure roller hardness during microfinishing. Analysis of the contact conditions and the surface roughness achieved). wt Werkstattstechnik Online 2017;107(1/2):59–65 (2017).
[39] Liang K, Angelopoulos S, Lepipas G, Tsarabaris P, Ktena A, Bi X, et al. Sensor to monitor localized stresses on steel surfaces using the magnetostrictive delay line technique. Sensors 2019;19(21):1–14.
[40] Ramirez-Rico J, Lee S-Y, Ling J, Noyan I. Stress measurement using area detectors: a theoretical and experimental comparison of different methods in ferritic steel using a portable X-ray apparatus. J Mater Sci 2016;51(11):5343–55.
[41] Kamada Y, Sasahara H. Residual stress fluctuates periodically via the workpiece rotation phase during low frequency vibration cutting. Precis Eng 2021;72:583–94.